Geology

Multi-scale stochastic modelling of ore textures at the George Fisher mine, Queensland, Australia

A. Richmond*, Golder Associates, Brisbane, Queensland, Australia, and
R. Dimitrakopoulos*, McGill University, Montreal, Quebec

KEYWORDS: Stochastic spatial simulation, Ore texture, Ore reserves.

Paper reviewed and approved for publication by the Geological Society of CIM.

ABSTRACT

The link between ore texture and mineral liberation has previously been established at a microscopic scale. To construct ore texture models that can be used in mining applications requires this relationship to be retained at a significantly larger scale. This is initially dealt with by finding a basic set of microtextures that form the elements of the ore textures at the next larger mesoscopic scale, simulating these mesotextures at a fine scale, then changing the support of the mesotexture simulations to generate the expected mining block/stope mesotexture distributions. Thus, a mutually exclusive and exhaustive set of spatially locatable mesotextures can be used to fully characterize the metallurgical properties of in situ material.

A method that generates expected distributions of mesotextures for any mining block size or shape is proposed, and includes: (1) characterizing the spatial correlation of the set of mesotextures with a single covariance function; (2) generating multiple simulations of mesotextures at a fine scale; and (3) using the simulations at a fine scale to generate the expected mining block/stope mesotexture distributions. A case study, using the George Fisher sediment-hosted base metal deposit in Queensland, Australia, is developed to demonstrate the proposed methodology as well as show the inadequacy of off-the-shelf approaches.

Mining-scale texture models can be used to improve the in situ discrimination of ore from waste by exploiting the joint spatial variability of grades and textures to quantify the expected metal recovery of in situ material, then calculate local marginal cut-off grades. An artificial case study is presented to demonstrate the changes in ore/waste selection when considering ore texture models compared to constant metal recoveries.

Introduction

The design and operation of ore processing plants can be enhanced by taking into account complex ore processing parameters, such as mineralogy, grindability, liberation, washability, pulp fluidity, density, and floatability. These parameters collectively characterize the metallurgical behaviour of the ore. However, even with the most sophisticated plant control system and mining practices, a response lag occurs between the measurement of an ore processing parameter and the corrective action required to be implemented. For example, Robertson and Sehic (1993) describe an ore control system at the Ok Tedi mine, Papua New Guinea, in which the downstream mill performance is radioed hourly to the pit geologist to enable more selective in-pit mining based on geological observations. It is during this lag time that an opportunity exists to maximize the profit of the resource by introducing a predictive ore control strategy.

Numerous authors have discussed the link between ore texture and metallurgical behaviour (Gaspar and Pinto, 1991; Blaschke and Siwiec, 1993; Ferrara et al., 1993; Kahn, 1993; King and Schneider, 1993; Bojevski et al., 1998). If the metallurgical properties of ore and the ore's texture are intimately linked, then the time-dependent variability of ore behaviour in the mill feed is directly related to the space-dependent variability of textures in the orebody, which is an intrinsic feature of the orebody. If these ore textures can be recognized, measured, and quantified in spatial models, then these ore texture models can form the basis for predicting, simulating, and controlling the time-dependent variability of the ore behaviour in the mill feed. Furthermore, if different metal recoveries are associated with the various ore textures, then spatial ore texture models, when combined with models of grades, can be used to enhance ore/waste delineation by defining local cut-off grades.

This paper presents a method to construct mining-scale models of ore texture distributions that involves: (1) defining ore textures at a practical scale; (2) characterizing the spatial ore texture continuity; (3) simulating the ore textures at a fine scale; and (4) using the fine scale ore texture models to characterize the texture distribution at the mining scale. The application of the method is shown for the George Fisher mine, Queensland, Australia. In addition, the influence of these texture models on ore/waste discrimination is discussed.

Modelling Ore Textures

The term 'ore texture' carries a variety of connotations for those in the mineral industry. A comprehensive review of the variations in the definition of ore texture is contained in Vink (1997). In this paper, ore texture refers to the mineral assemblage present, their volume fractions, the grain size, shape, and spatial distribution of each mineral phase, and the intergranular relationships.

A number of issues need to be addressed in the modelling of ore textures for mining applications, including: (1) the scale of the ore texture data; (2) how to classify or represent

* Formerly with WH Bryan Mining Geology Research Centre, The University of Queensland, Brisbane, Queensland, Australia

Andrew Richmond is a senior geostatistician working for Golder Associates, Brisbane, Australia. He obtained his Ph.D. in mining engineering (2003) from Imperial College, London, and his M.Sc. in geostatistics (1999) from The University of Queensland, Brisbane. He has worked as a consultant to the mining and finance industries with his company GeoRisk prior to joining Golder Associates. He has also worked for WH Bryan Mining Geology Research Centre, The University of Queensland, and Ross Mining.

Roussos Dimitrakopoulos holds the Canada Research Chair in sustainable mineral resource development and optimization under uncertainty and BHP Billiton Chair in mine planning optimization at McGill University. He undertakes this position after nearly a decade as professor and director, WH Bryan Mining & Geology Research Centre, University of Queensland. He obtained a Ph.D. in geostatistics from Ecole Polytechnique, Montreal, and a M.Sc. from the University of Alberta, Edmonton. He has worked and taught in Australia, North America, South America, Europe, the Middle East, South Africa, and Japan.

ore texture information; and (3) a methodology for modelling ore textures at a mining scale.

The earlier definition of ore texture does not place any constraint on the scale at which ore textures can be defined. Three scales are commonly referred to in the mining community: microscopic (grain-scale), mesoscopic (hand specimen), and macroscopic (mappable unit). The existence of ore textures at different scales can be dealt with by finding a basic set of ore textures at the microscopic scale that form the elements of the ore textures at the next larger mesoscopic scale. A group of ore textures defined at this mesoscopic scale constitutes an ore type which may be a mappable unit. In this paper, the terms 'microtexture' and 'mesotexture' are defined to represent ore textures at the microscopic and mesoscopic scales, respectively. Ore texture is now used as a generic term that refers to ore textures on all scales inclusively.

Comprehensive classifications for ore textures have previously been established. For example, Ramdohr (1980) proposed guidelines for texture description and classification. Three approaches to texture classification are used in the literature: (1) a purely descriptive classification; (2) a genetic classification based on assumptions on the formation of deposits; and (3) a technical classification, generally based on physical or chemical criteria (Vink, 1997). None of these approaches adequately describe all properties of the rock, based on a strict interpretation of the definition of ore texture. Vink (1997) proposed a microtexture and mesotexture classification scheme, specific to the George Fisher mine that completely characterizes the occurrence of all minerals in the rock. The mesotexture classification provides a framework for representing rock material at a scale that can be used in traditional methods of modelling categorical variables.

Modelling of ore mesotextures at a scale practical for mining applications is based on three factors: (1) characterization of the spatial mesotexture continuity; (2) conditional simulation of mesotextures at a fine scale; and (3) use of fine-scale mesotexture models to generate mesotexture distributions at the scale of mining.

Spatial Structures

Consider K mutually exclusive and exhaustive mesotextures, k = 1,...,K. An indicator transform for a particular mesotexture s_k at a sample location x in a mineral deposit is given by:

$$i(x; s_k) = \begin{cases} 1 & \text{if location x belongs to mesotexture } s_k \\ 0 & \text{otherwise} \end{cases} \quad \ldots\ldots(1)$$

Thus, the sampled mesotexture data can be coded into K indicator datasets $\{i(x;s_k), k=1,\ldots,K\}$. To quantify the spatial variability of the K mesotextures, a multi-texture covariance function is used. The multi-texture or phase covariance $C_M(H)$ proposed by Soares (1992) measures the chances that two points separated by vector h belong to the same mesotexture and is given by:

$$C_M(h) = \frac{1}{KN(h)} \sum_{k=1}^{K} \sum_{j=1}^{N} i(x_j;s_k) \cdot i(x_j + h;s_k) - p_{-h}(s_k) \cdot p_{+h}(s_k) \quad \ldots\ldots\ldots\ldots\ldots\ldots(2)$$

where N(h) is the number of pairs for separation vector h, $p_{-h}(s_k)$ is the proportion of tail samples that are mesotexture s_k, and $p_{+h}(s_k)$ is the proportion of head samples that are mesotexture s_k.

The multi-texture correlogram $\rho_M(h)$ is a standardized form of the multi-texture covariance, calculated as:

$$\rho_M(h) = \frac{C_M(h)}{\sum_{k=1}^{K} \sigma^2_{|h|}(s_k)} \quad \ldots\ldots\ldots\ldots\ldots (3)$$

where $\sigma^2_{|h|}(s_k) = p_{|h|}(s_k) - p^2_{|h|}(s_k)$, the variance of the indicators for mesotexture s_k.

The multi-texture correlogram in equation 3 is a correlogram that incorporates all K mesotextures in a single measure of spatial variation. Although equation 3 is an average type indicator correlogram of the K mesotextures, the multi-texture correlogram is not derived from averaging the K indicator correlograms at each separation vector h.

Conditional Simulation of Mesotextures

Modelling of categorical variables, such as mesotextures, by stochastic simulation methods has been demonstrated in various studies (Soares, 1992; Yarus and Chambers, 1994; Goovaerts, 1996). For the simulation of ore mesotextures, a new sequential "growth" algorithm extending the off-the-shelf sequential indicator simulation (SIS) (Alabert, 1987; Goovaerts, 1997) is used herein. The method mimics a natural process of "informed" growth in a spatial pattern and generates geologically plausible patterns (Richmond, 1998; Richmond and Dimitrakopoulos, 2000). The SIS algorithm with sequential growth or controlled paths is:

- use a controlled simulation path, select a location x at which no mesotexture exists;
- estimate the local conditional cumulative distribution function *(ccdf)* of the K mesotextures at x using point kriging of the K indicator datasets, a correction to local probabilities, and the multi-texture correlogram;
- draw a random number n uniformly distributed in [0,1], then the interval of the local *ccdf* in which n falls is the mesotexture simulated at location x;
- add the simulated mesotexture to the K conditioning indicator datasets;
- repeat steps 1 to 4 following controlled paths selected until all locations have been allocated a mesotexture; and
- generate additional equally probable models of mesotextures by following the entire sequential procedure with a different controlled path.

Successive growth or controlled simulation paths involve defining a set of conditions that, if met when location x is visited randomly, allows a mesotexture to be simulated at x. If the conditions are not met, then the location is not considered until the conditions are changed. By relaxing the conditions for subsequent random visits, mesotextures are simulated at all locations. The condition used is distance from the existing data. This distance is relaxed in a sequence of 'passes' or steps needed to complete the process.

At a given iteration step t, a deviation exists between the target proportion of mesotexture s_k within the study area A, $p(s_k;A)$, and the corresponding simulated proportion of mesotexture s_k at t, $p^t(s_k;A)$. The mesotexture probabilities estimated by point kriging $p^*(s_k;x)$ are corrected (for details see Richmond and Dimitrakopoulos, 2000) by this deviation prior to building the local *ccdf* of the K mesotextures (Soares, 1998), i.e.:

$$p^{*t}(s_k;x) = p^*(s_k;x) + \left[p(s_k;A) - p^t(s_k;A)\right] \quad \ldots\ldots (4)$$

Each simulation of mesotextures generated by modified SIS above honours the sampled mesotexture data, the global mesotexture statistics, and the multi-texture correlogram. Differences between models reflect the uncertainty of the mesotextures simulated. Local uncertainty measures may be provided by the entropy of the local *ccdf* built from multiple simulated mesotexture models (Goovaerts, 1997), calculated as:

$$H(x) \circ - \sum_{k=1}^{K} [\ln p^*(x;s_k)] \cdot p^*(x;s_k) \geq 0 \quad \ldots\ldots\ldots (5)$$

where $p^*(x;s_k)$ is the proportion of mesotextures simulated at x that are s_k. At any datum location the probability is one for the prevailing mesotexture, hence, H(x) is 0. For all other locations the measure H(x) falls in the interval

[0, lnK]. The upper bound lnK is associated to the uniform distribution, where $p^*(x;s_k) = 1/k$, $\forall k$. Therefore, a standardized measure of local entropy is:

$$H_R(x) = \frac{H(x)}{\ln K} \in [0,1] \quad \ldots\ldots\ldots\ldots (6)$$

Mesotexture Models at the Mining Scale

Classifying a mining-scale block with a single mesotexture is highly practical for mining purposes. Previous studies have investigated allocating a location (Soares, 1992; Goovaerts, 1996) or mining-scale block (Richmond and Dimitrakopoulos, 1997; Richmond, 1998) to the category with the largest local proportion under various constraints. In all of these studies, significant local bias was introduced, and poor reproduction of either the target global proportions or the transitional statistics resulted.

The straightforward combination of the simulated mesotextures from multiple realizations to produce the expected mining block/stope mesotexture distributions is shown in Figure 1. This approach to generating models of mesotexture distributions of mining blocks from mesotexture simulations at the data scale is unbiased, and the size and shape of the blocks do not have to be regular, as shown in Figure 1.

Simulating Mesotextures at the George Fisher Deposit

To illustrate the proposed methodology, an example of modelling mesotextures for a fan of drill holes at the George Fisher massive sulphide deposit located in the historic mining region of Mount Isa in Queensland, Australia, is presented in this section. The George Fisher mine is one of the largest undeveloped lead-zinc deposits in the world with ore production in the order of 3 mt/yr. George Fisher is owned and operated by Xstrata (previously Mount Isa Mines).

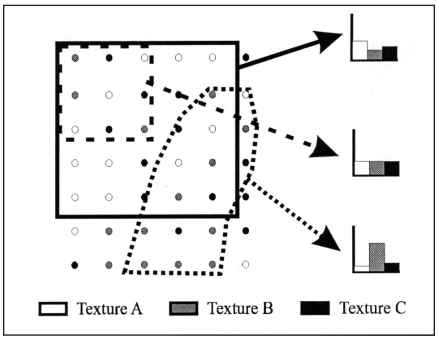

Fig. 1. Schematic representation of how the proposed upscaling approach can incorporate blocks of any size and/or shape.

Geology and Mineralization

The George Fisher mine is situated approximately 20 km north of Mount Isa within deformed sediments of the Urquhart Shale, which is part of the Mount Isa Group. A simplified geological interpretation of the George Fisher mine is shown in Figure 2. The sedimentary units in this diagram dip steeply to the west at 60° to 70°, unless deformed by tectonic activity. The Urquhart Shale hosts all known economic silver-lead-zinc mineralization and is mostly concordant to the sedimentary bedding. The drill holes used in this study were collared in footwall pyritic shales of the Urquhart Shale and directed stratigraphically upwards, shown in Figure 2.

Ore Texture Data

At the George Fisher deposit, the link between ore texture and metallurgical properties for a set of 10 mutually exclusive and exhaustive mesotextures is well established and economically significant (Vink, 1997; Bojevski et al., 1998). This metallurgical relationship relies on a basic set of microtextures that form the elements of the textures at the next larger mesoscopic scale, which are logged in diamond core as discrete mesotextures.

The mesotextures used in this study and their characteristics are shown in Table 1. In this table, banded mesotextures consist of alternating bands of sulphide-rich and sulphide-poor shale, in which the sulphide mineralization is fine grained (<30 microns). Massive mesotextures are coarser grained aggregates of sulphide mineralization that may contain isolated fragments of carbonaceous shale with remnant banded mesotextures. Some of the meso/microtexture relationships are shown in Figure 3, which includes photographs of two mesotextures at the core scale and photomicrographs of their corresponding microtexture compositions. In this figure, the relative difference in grain size between banded mesotextures and massive mesotextures is visible by comparing, for instance, Figures 3b and 3d.

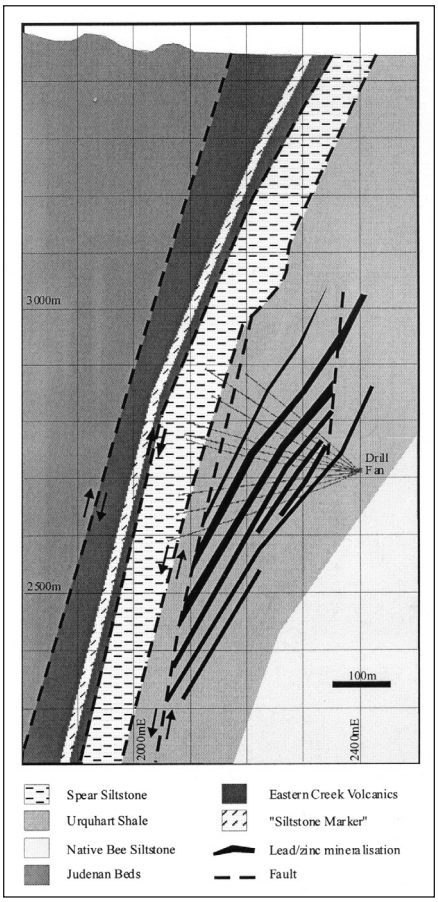

Fig. 2. East-west section through the George Fisher mine, Queensland, Australia, at approximately 7020 N showing a simplified geological interpretation.

As detailed in Richmond (1998), mesotextural logging and data processing included: (1) recording the proportions of each small-scale mesotexture within larger-scale drill hole intervals; (2) compositing to small intervals; and (3) declustering to establish representative global mesotexture proportions.

The downhole logs of mesotexture proportions are shown in Figure 4; the sample size is 0.1 m. In this diagram, all 10 mesotexture proportions vary significantly throughout the study area. For example, Mesotexture 7 was commonly intersected in the deeper parts of the drill holes, but rarely near the drill hole collars.

Table 1. Mesotexture categories used in this study and their characteristics

Number	Mesotexture Name	Prop. (%)	Description
1	Banded pyrite	16.78	Banded mesotexture with 100% of the sulphide minerals pyrite ± pyrrhotite
2	Banded pyrite-sphalerite	3.38	Banded mesotexture with sphalerite >0% and <50% of the sulphide minerals
3	Banded sphalerite	1.82	Banded mesotexture with sphalerite ≥50% of the sulphide minerals
4	Massive galena	1.06	Massive mesotexture with galena >60% of the sulphide minerals
5	Massive sphalerite-galena	0.92	Massive mesotexture with approximately equal proportions of sphalerite and galena
6	Massive sphalerite	1.49	Massive mesotexture with sphalerite >60% of the sulphide minerals
7	Massive pyrite	3.42	Massive mesotexture with 100% of the sulphide minerals pyrite ± pyrrhotite
8	Massive pyrrhotite	0.14	Massive mesotexture with 100% of the sulphide minerals pyrrhotite ± pyrite
9	Banded pyrrhotite	0.08	Banded mesotexture with 100% of sulphides pyrrhotite ± pyrite
10	Gangue	70.92	100% carbonaceous or calcareous shale/siltstone

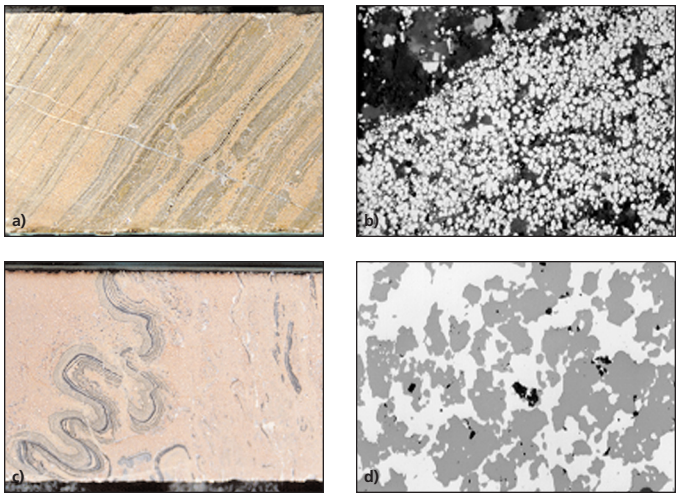

Fig. 3. Texture photographs and photomicrographs: (a) banded pyrite at drill core scale; (b) banded pyrite at microscopic scale (fine-grained pyrite is white and gangue is black); (c) massive sphalerite-galena at drill core scale showing remnant banded pyrite (folded); (d) massive sphalerite-galena at microscopic scale (galena is white, sphalerite is grey, and gangue is black). Note that all scales are approximate.

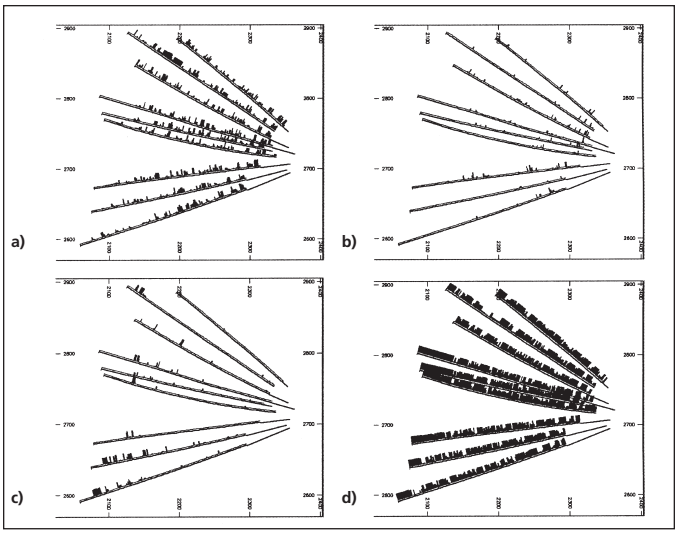

Fig. 4. Down hole logs of mesotexture proportions (0.1 m samples): (a) mesotexture 1 (declustered global proportion = 16.78%); (b) mesotexture 3 (1.82%); (c) mesotexture 7 (3.42%); and (d) mesotexture 10 (70.92%).

Spatial Structures of Mesotextures

To implement the method proposed in the previous section, directional experimental multi-texture correlograms are first calculated then a suitable model fitted. The experimental and modelled multi-texture correlograms are shown in Figure 5. This diagram includes indicator correlograms of mesotextures, which are erratic due to highly variable global proportions and the sparse data configuration. Note that the multi-texture correlogram is not the average of the 10 indicator correlograms of mesotextures. The model fitted is spherical (sph) as shown below:

$$\rho(h) = 1.0 - \left[0.25 + 0.45\,\mathrm{sph}\left(\sqrt{\left(\frac{h_{30°\text{-}90°}}{1.0}\right)^2 + \left(\frac{h_{60°\text{-}270°}}{3.0}\right)^2}\right) + 0.30\,\mathrm{sph}\left(\sqrt{\left(\frac{h_{30°\text{-}90°}}{5.0}\right)^2 + \left(\frac{h_{60°\text{-}270°}}{35.0}\right)^2}\right)\right] \quad \ldots\ldots (7)$$

Conditional Simulation of Mesotextures

Initial mesotexture simulations generated with the traditional, off-the-shelf SIS algorithm as implemented in Deutsch and Journel (1998) did not produce geologically realistic patterns representing the observed ore texture patterns at the mine site and were discarded by the mine's geologists. In addition, the simulated mesotextures failed to reproduce the target mesotexture proportions and mesotexture spatial structures. Figure 6 shows one simulated model of textures using the traditional SIS method. The sequential simulation framework has no constraints on the order in which locations are simulated, however, it was observed that control over the path used to sequentially simulate grid nodes could be used to generate geologically representative mesotexture realizations.

The growth-based SIS algorithm presented earlier was used to generate 20 realizations on a fine grid, based on the available data

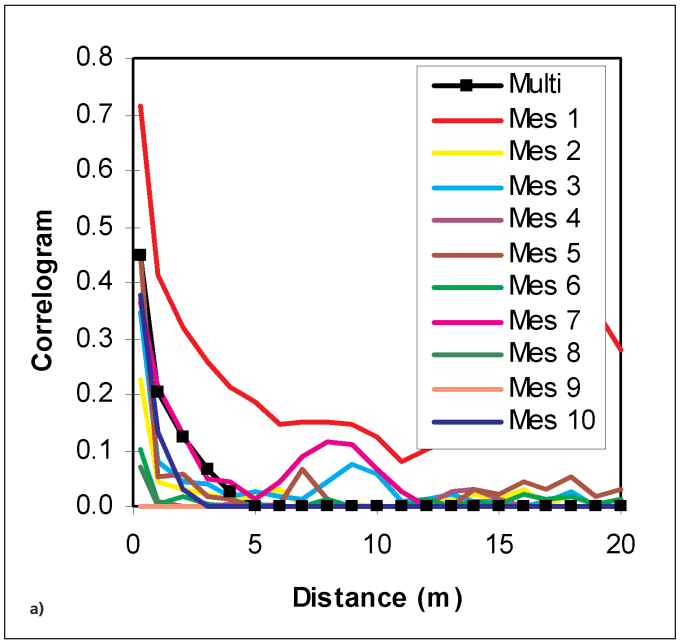

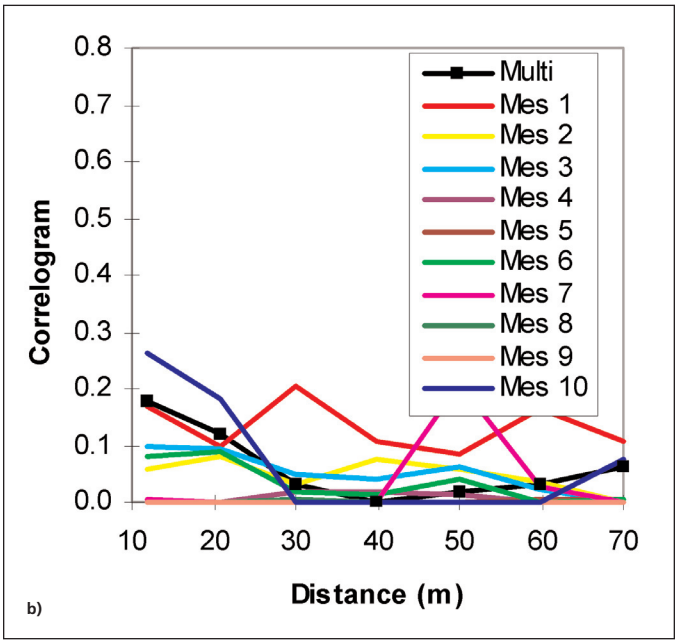

Fig. 5. Experimental multi-texture and indicator correlograms: (a) 30° to 90°, and (b) 60° to 270°. Multi = multi-texture correlogram; Mes 1 = indicator correlogram for mesotexture 1.

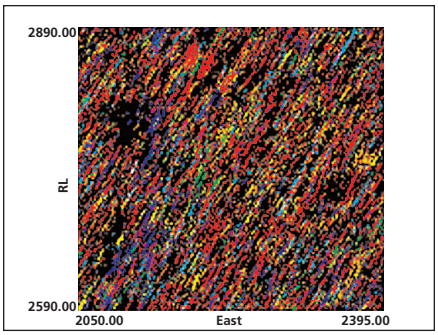

Fig. 6. A realization of mesotextures generated with the traditional "off-the-shelf" sequential indicator simulation algorithm (see Fig. 4 for drill hole locations).

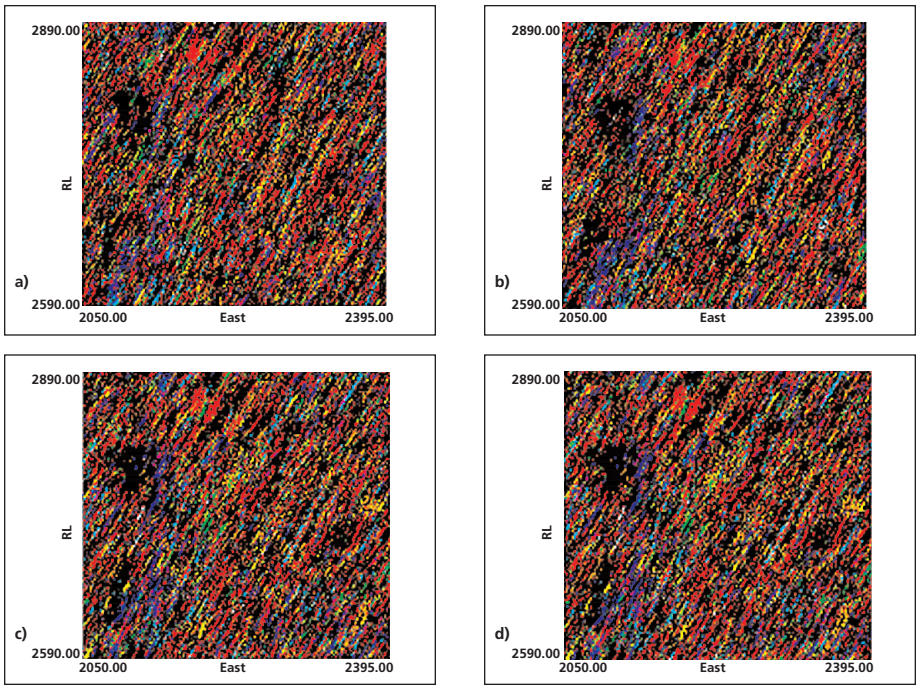

Fig. 7. Realizations of mesotextures generated with the modified sequential indicator simulation with growth or control path (see Fig. 4 for drill hole locations).

and the covariance function in equation 7. Four of these realizations are shown in Figure 7. In this diagram, all four realizations display similar characteristics close to the drill fan where there is conditioning data. For example, an area dominated by Mesotexture 10 appears in the top left corner of all the realizations. In the top right and bottom right parts of the realizations, which is remote from the drill fan conditioning data, they vary in appearance, which reflects the uncertainty of the mesotextures simulated at these locations. Near the origin of the drill fan, in the centre right part of the simulations, there are narrow zones consisting mostly of mesotextures 1, 2, and 3 dipping steeply to the west at ±60° separated by areas consisting entirely of Mesotexture 10. This reflects a series of discrete mineralized lenses dominated by banded mesotextures that are separated by unmineralized gangue (Mesotexture 10).

Validation of the mesotexture simulations involved checking with mine geologists that the realizations of simulated mesotextures were realistic, and then checking the reproduction of the experimental global mesotexture proportions and several measures of spatial continuity. Figure 8 shows the multi-texture model used for simulating mesotextures and the corresponding correlograms calculated from the 20 realizations. In this figure, there is close match between all multi-texture correlograms calculated from the simulations and the model. The univariate and bivariate measures of spatial continuity must also be checked to ensure reasonable reproduction of the experimental indicator and cross-indicator correlograms.

Local Uncertainty of Simulated Mesotextures

Local uncertainty measures were calculated for the mesotexture simulations using equation 6 and are displayed in Figure 9. In this figure, the location of the drill fan conditioning data is clearly visible. Near the origin of the drill fan there are several narrow zones of low entropy dipping steeply to the west at approximately 60°, separated by areas of higher entropy. These zones of low and high entropy reflect logged zones containing a single mesotexture category (unmineralized gangue) and multiple mesotexture categories (associated with mineralized lenses), respectively. In Figure 9, high values of entropy are observed even at data proximity. These high values may reflect the possibility that a few different mesotextures are equally probable. Note that with two to five equally probable mesotextures, the standardized entropies are 0.31, 0.48, and 0.70, respectively. The uncertainty described here is not the same type of uncertainty as the uncertainty far from data locations, where one has no understanding about possible ore textures. Areas distant to the conditioning data, for example, in the lower right and top right areas of Figure 9, have relatively high local

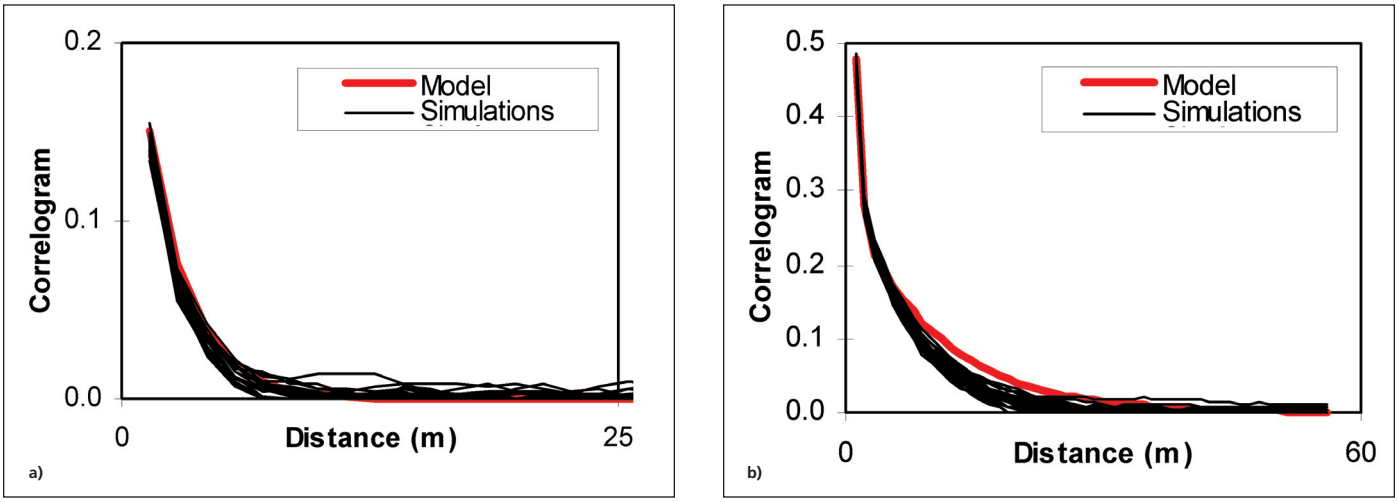

Fig. 8. Multi-texture correlograms for 20 mesotexture simulations: (a) 45° to 90°, and (b) 60° to 270°.

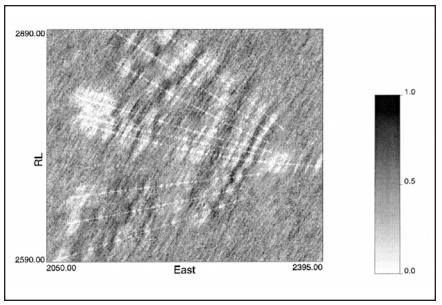

Fig. 9. Standardized entropy of the local conditional cdf of mesotexture probabilities.

uncertainty values, which may suggest that more than 20 realizations should be used for entropy calculations. Nevertheless, standardized entropy calculations in Figure 9 show cases where high entropy, implying high uncertainty, appears close to data rather than far from the data. This is possible and it attempts to account for local variability in addition to data proximity. However, entropy measures in this example also demonstrate a level of ambiguity that needs to be further understood.

From Mesotexture Simulations to Texture Distributions for Mining Blocks

The next step is to determine the expected mesotexture distributions for given block sizes. Figure 10 shows the mesotexture proportions for 10 m by 10 m blocks. Blocks near the drill fan display close relatationships between block proportions and drill hole intersections of the corresponding mesotexture, shown in Figure 4. Blocks that are distant to the conditioning data fluctuate more closely about the experimental global mesotexture proportions. For example, in the top righthand corner of Figure 10, the block proportions for Mesotexture 1 vary from 12% to 22%, while near the drill fan, the block proportions range from 5% to 80%. The experimental global proportion of Mesotexture 1 is 16.78%.

Influence of Ore Textures on Ore/Waste Delineation

Traditional methods of outlining ore involve the application of a single cut-off grade, based on a fixed recovery factor, to the in situ expected grade. The mining-scale ore texture distributions can aid the in situ discrimination of ore from waste. This could involve exploiting the joint spatial variability of grades and textures to quantify the expected metal recovery of in situ material, then calculate local marginal cut-off grades.

The Expected Metal Recovery of In Situ Material

If the ore's texture and its metal recovery are intimately linked, then the expected distributions of ore textures can be used to calculate the expected metal recovery as:

$$r_b = \frac{\sum_{\alpha=1}^{G}\sum_{l=1}^{L} r_k(x^l_\alpha)\cdot z(x^l_\alpha)}{\sum_{\alpha=1}^{G}\sum_{l=1}^{L} z(x^l_\alpha)} \quad \ldots\ldots\ldots (8)$$

where r_b is the fractional metal recovery for mining block b, G is the number of grid nodes located within b, L is the number of realizations, $r_k(x^l_\alpha)$ is the fractional metal recovery for mesotexture s_k, simulated at x_α on the l^{th} realization, and $z(x^l_\alpha)$ is the metal grade simulated at x_α on the l^{th} realization.

The simulated metal grades must honour the transitional statistics between ore textures and metal grades separated by a vector $h = 0$. For example, if a massive galena ore texture was simulated at x_α, then a co-existing lead grade of 0% at x_α is unrealistic, and a low lead grade is unlikely. Alternatively, if gangue is simulated at a location all economic metal values must be 0%. In theory, the transitional statistics between ore textures and metal grades should be honoured for all h that belong to the deposit area.

It is important to note that the expected metal recovery for a block of ore, calculated with equation 8, is sensitive to: (1) the number of ore texture-grade co-simulations L; (2) the mining selectivity; and (3) the ore processing method employed. The impact of mining selectivity on the expected metal recovery depends on the short-scale variability and connectivity of the ore textures and grades.

Local Marginal Cut-off Grades

The marginal cut-off grade of a deposit may be calculated as:

$$z^b_c = \frac{c_o - c_w}{p \cdot r_b} \quad \ldots\ldots\ldots\ldots (9)$$

where z^b_c is the marginal cut-off grade for mining block b, c_o is the mining and processing cost per ton of ore, c_w is the mining cost per ton of waste, and p is the metal price per concentration unit, and r_b is the fractional metal recovery associated with processing.

In the previous section, the distribution of ore textures was heterogeneous, thus r_b, and consequently z^b_c, may vary in space. These local marginal cut-off grades can be used to improve the in situ discrimination of ore from waste.

An Artificial Example

Consider the artificial example, shown in Figure 11, of three mesotextures that display different metallurgical characteristics, for which the expected block mesotexture proportions are known. This example could represent mesotexture data from a sedimentary-hosted base metal deposit such as the George Fisher deposit, with A being coarse-grained sphalerite and galena mineralization, B being fine-grained pyrite and sphalerite mineralization, and C being fine-grained sphalerite mineralization. Metal recovery from material composed entirely of Mesotexture A is 81%, mesotexture B, 55%, and Mesotexture C, 77%. The global

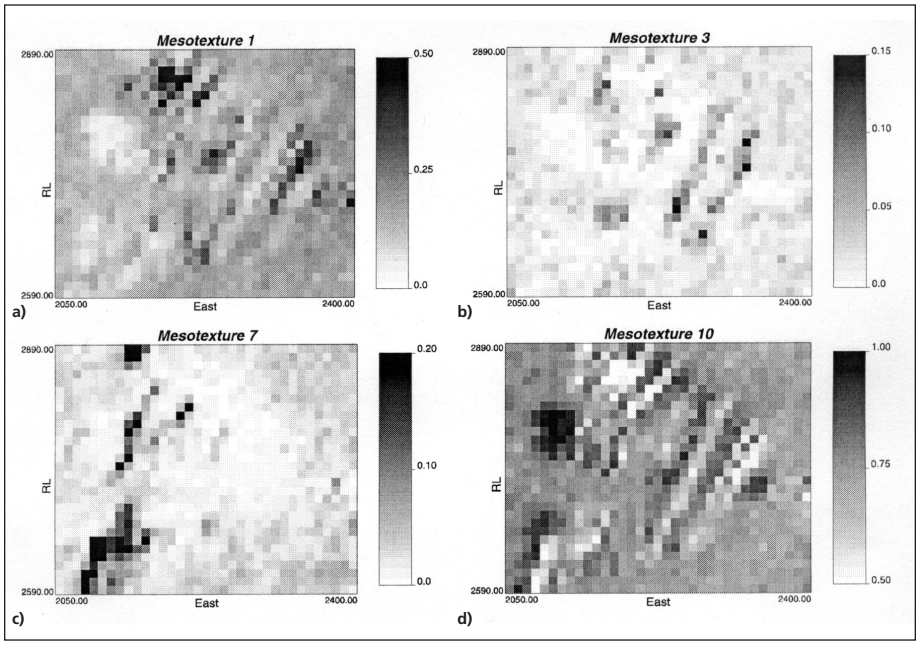

Fig. 10. Mesotexture proportions for 10 m by 10 m blocks.

proportions of Mesotextures A, B, and C are 40%, 16.4%, and 43.6%, respectively.

Based on the global mesotexture proportions and the metal recoveries associated with each mesotexture, the average metal recovery is 75%. The net value of a block of material is the extractable metal value minus the mining and milling costs. If the net value is positive the block is ore, otherwise it is waste. Figure 12 shows the block net values and the block ore/waste classification based on the economic parameters included in the diagram. In this diagram, the bottom westernmost block has a net value of -$933 and is classified as waste. The ore/waste classification is based on all blocks being metallurgically identical and, consequently, the ore/waste discrimination is simply related to the interpolated grade.

If we assume that the metal grades are constant within a block, then the metal recoveries calculated from equation 8 are related solely to the proportions of the three mesotexture types within a block, shown in Figure 11. If the metallurgical recoveries based on the ore texture distributions are combined with the interpolated grades, the re-evaluation of the blocks in the example changes the ore/waste boundary. This is shown in Figure 13 where the net value of the same blocks in Figure 12 may change significantly when texture information is considered. Some of the blocks that were previously considered to be ore are now classified as waste and vice versa. In Figure 13, note that the net value of the bottom westernmost block is now $1,119 and classified as ore. Similarly, a block in the lower right part of the figure has changed from ore to waste with a negative net value when considering both grade and texture information.

Comments and Conclusions

In the case study at George Fisher, the existence of ore textures at different scales is dealt with by finding a basic set of ore textures at the microscopic scale that form the elements of the ore textures at the next larger mesoscopic scale, which can be logged in diamond core as discrete mesotextures. The approach to ore texture modelling described in this paper generates expected distributions of mesotextures for any block size or shape from fine-scale mesotexture simulations.

The modified SIS algorithm with sequential growth or controlled paths generated mesotexture realizations that are visually realistic, and honour the global univariate and bivariate data statistics. Other techniques such as pluriGaussian truncated simulation (Le Loc'h and Galli, 1997), sequential modelling of relative indicator variables (Dimitrakopoulos and Dagbert, 1993) or the successive co-indicator simulation approach (Vargas-Guzman and Dimitrakopoulos, 2003) may be appropriate for simulating mesotextures.

The standardized entropy of the *ccdf* of simulated mesotextures demonstrates the uncertainty of a mesotexture simulated at a location. This measure of uncertainty attempts to reflect both the structural distance to sampled data locations and the variability of the experimental data within the local neighbourhood. However, it may also be ambiguous and needs to be further understood.

The economic benefit from modelling ore textures is, in part, related to the integrity of the texture models at the mining scale. The question of scale and when to upscale during the data acquisition, compositing, and texture modelling process is critical in honouring the local and global texture statistics, and the texture spatial structures. It is easy to misrepresent ore textures in large blocks or stopes, either by upscaling texture data early in the modelling process, or by upscaling in an inappropriate manner.

Geostatistical techniques have been widely used for evaluating ore reserves, quantifying the effects of different mining strategies, and evaluating the variability of the expected mill feed head-grade. This paper discussed the influence of texture models on in situ ore/waste delineation. However, the texture models can also form the basis for predicting, simulating, and controlling the time-dependent variability of the ore behaviour in the mill feed.

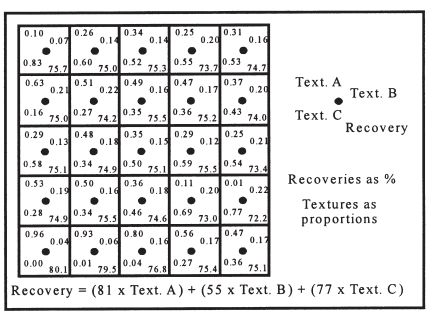

Fig. 11. Mesotexture proportions for a number of blocks.

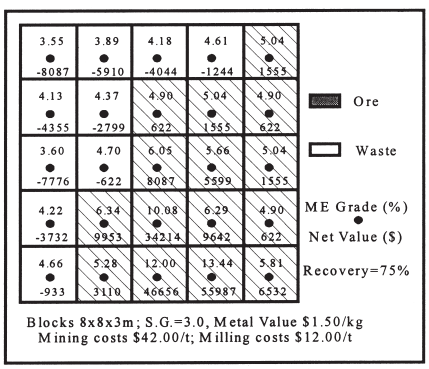

Fig. 12. Net value of blocks if mined and processed using a fixed recovery.

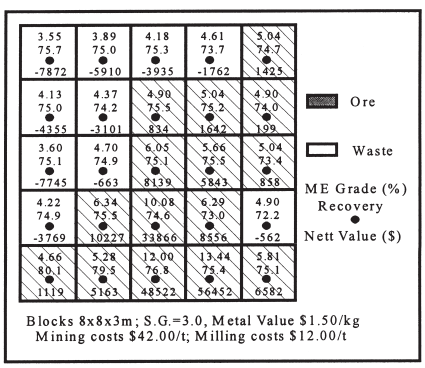

Fig. 13. Net value of blocks if mined and processed incorporating both grade and ore texture information.

Acknowledgments

Thanks are in order to Mount Isa Mines Ltd. and the staff of the George Fisher mine, Queensland, Australia, for collaboration, data, and funding. The Corporate Research Centre for Mining Technology and Equipment, as well as the WH Bryan Mining Geology Research Centre, The University of Queensland, Australia, provided additional funding. The comments of anonymous reviewers assisted with the improvement of the manuscript.

References

ALABERT, F., 1987. Stochastic Imaging of Spatial Distributions using Hard and Soft Information. M.Sc. thesis, Stanford University, Department of Applied Earth Sciences, Stanford, California, 168 p.

BLASCHKE, Z. and SIWIEC, A., 1993. Evaluation of mineral processing effectiveness and causes of mineral losses. Proceedings, XVIII International Mineral Processing Congress. Australasian Institute of Mining and Metallurgy, p. 491-495.

BOJEVSKI, D., VINK, L., JOHNSON, L.W., LANDMARK, V., JOHNSON, M., MACKENZIE, J., and YOUNG, M.F., 1998. Metallurgical characterization of George Fisher ore textures and implications of ore processing. *In* Mine to Mill. The Australasian Institute of Mining and Metallurgy, Brisbane, Queensland, p. 88-94.

DEUTSCH, C.V. and JOURNEL, A.G., 1998. GSLIB: Geostatistical Software Library and User's Guide. Oxford University Press, New York, 340 p.

DIMITRAKOPOULOS, R. and DAGBERT, M., 1993. Sequential modelling of relative indicator variables: Dealing with multiple lithology types. *In* Geostatistics — Troia'92. *Edited by* A. Soares. Kluwer Academic Publishers, p. 413-424.

FERRARA, G., GUARASCIO, M., and MASSACCI, P., 1993. Mineral processing design and simulation using geostatistical modelling of ore characteristics. Proceedings, XVIII International Mineral Processing Congress. Australasian Institute of Mining and Metallurgy, p. 497-503.

GASPAR, O. and PINTO, A. 1991. The ore textures of the Neves-Corvo volcanogenic massive sulphides and their implications for ore beneficiation. Mineralogical Magazine, 55, p. 417-422.

GOOVAERTS, P., 1996. Stochastic simulation of categorical variables using a classification algorithm and simulated annealing. Mathematical Geology, 28, p. 909-921.

GOOVAERTS, P., 1997. Geostatistics for Natural Resources Evaluation. Oxford University Press, New York, 483 p.

KAHN, H., 1993. Applied mineralogical studies on the complex Pitinga primary ore, Brazil — Cryolite, Sn, Nb, Zr, and REE. Proceedings, ICAM 1993. International Council for Applied Mineralogy, p. 272-274.

KING, R.P. and SCHNEIDER, C.L., 1993. Mineral liberation in continuous milling circuits. Proceedings, XVIII International Mineral Processing Congress. Australasian Institute of Mining and Metallurgy, p. 203-211.

LE LOC'H, G. and GALLI, A., 1997. Truncated plurigaussian method: theoretical and practical points of view. *In* Geostatistics — Wollongong'96. *Edited by* E. Baafi and N. Schofield. Kluwer Academic Publishers, Wollongong, New South Wales, Australia, p. 211-222.

RAMDOHR, P., 1980. The Ore Minerals and their Intergrowths, 2nd Edition. Pergamon Press, Oxford, 1206 p.

RICHMOND, A.J., 1998. Multi-Scale Ore Texture Modelling for Mining Applications. M.Sc. thesis, The University of Queensland, WH Bryan Mining Geology Research Centre, Brisbane, Queensland, 190 p.

RICHMOND, A.J. and DIMITRAKOPOULOS, R., 1997. Geostatistical texture modelling in enhancing ore reserve estimation in base metal deposits. Proceedings, Third International Mining Geology Conference. Australasian Institute of Mining and Metallurgy, p. 99-103.

RICHMOND, A.J. and DIMITRAKOPOULOS, R., 2000. Evolution of a simulation: Implications for implementation, Volume 1. *In* Geostatistics 2000. *Edited by* W. Kleingeld and D. Krige. Geostatistical Association of South Africa, p. 134-144.

ROBERTSON, I.G. and SEHIC, O.A. 1993. Ore quality control for process optimization. Proceedings, International Mining Geology Conference. Australasian Institute of Mining and Metallurgy, p. 227-234.

SOARES, A., 1992. Geostatistical estimation of multiphase structures. Mathematical Geology, 24, p. 149-160.

SOARES, A., 1998. Sequential indicator simulation with correction for local probabilities. Mathematical Geology, 30, p. 761- 765.

VARGAS-GUZMAN, J.A. and DIMITRAKOPOULOS, R., 2003. Successive non-parametric estimation of conditional distributions. Mathematical Geology, 35, p. 39-52.

VINK, L., 1997. Textures of the Hilton North Deposit, Queensland, Australia, and their Relationship to Liberation. Ph.D. thesis, The University of Queensland, Brisbane, Queensland, 170 p.

YARUS, J.M. and CHAMBERS, R.L., 1994. Stochastic modeling and geostatitics. American Association of Petroleum Geologists, Tulsa, Oklahoma, 379 p.